Highlights

Reverse-Time Migration for Evaluating the Internal Structure of Tree-Trunks Using Ground-Penetrating Radar

- A processing framework for detecting tree decays in diseased trees.
- A real-field case study that demonstrates the capabilities of the suggested method.

Reverse-Time Migration for Evaluating the Internal Structure of Tree-Trunks Using Ground-Penetrating Radar

Amir M. Alani[1], Iraklis Giannakis[2], Lilong Zou[3], Livia Lantini[4] and Fabio Tosti[5]

[1] University of West London, School of Computing and Engineering, St Mary's Rd, Ealing, London W5 5RF. E-mail: amir.alani@uwl.ac.uk

[2] University of West London, School of Computing and Engineering, St Mary's Rd, Ealing, London W5 5RF. E-mail: iraklis.giannakis@uwl.ac.uk

[3] University of West London, School of Computing and Engineering, St Mary's Rd, Ealing, London W5 5RF. E-mail: lilong.zou@uwl.ac.uk

[4] University of West London, School of Computing and Engineering, St Mary's Rd, Ealing, London W5 5RF. E-mail: livia.lantini@uwl.ac.uk

[5] University of West London, School of Computing and Engineering, St Mary's Rd, Ealing, London W5 5RF. E-mail: fabio.tosti@uwl.ac.uk

Corresponding author: Iraklis Giannakis

E-mail: iraklis.giannakis@uwl.ac.uk

Keywords: Ground penetrating radar **(**GPR), tree health monitoring, migration, tree, decay, emerging infectious diseases (EIDs)

Abstract:

Modern socioeconomic factors such as global timber trade and international travelling have contributed to the rapid increase of Emerging Infectious Diseases (EIDs) of trees with devastating effects to the European forests and woodlands. To that extent, numerous non-destructive methodologies have been suggested as diagnostic tools in order to effectively monitor and maintain potential outbreaks. Ground-penetrating radar (GPR) is an appealing method for tree monitoring as it provides with a trivially deployable and efficient detection tool, suitable for large-scale forestry applications. Nonetheless, traditional GPR approaches are tuned for surface measurements and they are not compatible with the unique measurement configurations associated with forestry applications. Within that context, we present a novel-processing framework, which is capable of addressing features with irregular measurements on closed surfaces. A positioning method is described that exploits a wheel-measuring device in order to accurately associate each A-Scan with its corresponding coordinates. In addition, a processing pipeline is presented that aims at eliminating the ringing noise due to the layered nature of the trees. Lastly, a reverse-time migration is applied to the processed B-Scan in order to effectively map the reflectors present within the trunk. The suggested scheme is successfully tested in both numerical and real-field experiments, indicating the validity of the current approach.

1. Introduction

Emerging Infectious Diseases (EIDs) of trees -caused by pathogens, pests and fungi- pose a major threat for forests and woodlands [1], [2]. Recent outbreaks almost brought some species to extinction [3], [4] with devastating effects to the

74 European flora. It should be highlighted that from 1995-2010, a 13-fold increase
75 of EIDs has been recorded globally [2]. This rapid increase is due to anthropic
76 activities such as international travelling [2], global timber trade [1] and human
77 population increase [5]. Furthermore, climate change and the consequent rise of
78 the global temperature have added to this phenomenon [2].
79 Representative examples of recent outbreaks of EIDs are the ash dieback, the
80 acute oak decline (AOD) and the chestnut blight. Ash dieback is a prominent EID
81 that has invaded the United Kingdom (UK) in 2012 [1] and it has spread majorly
82 in central England and Wales [6]. Less than 5% of the ash trees are immune to
83 this disease and it is predicted that most of the ash trees in the UK are going to be
84 affected and die in the next twenty years [7]. AOD is a particularly aggressive
85 EID that can lead to tree mortality within a period of 3-5 years [8]. AOD has been
86 introduced to the UK in 2006 and since then has rapidly spread mostly in the
87 central part of England [9]. The effects of ash dieback and AOD to the forests and
88 woodlands of the UK resemblance the effects of chestnut blight to the chestnut
89 population in the North America during the last century [10]. Chestnut blight
90 accidentally invaded North America in 1904 and rapidly spread within the
91 following 40 years [10]. The nearly four billion chestnut population of North
92 America almost brought to extinction with just small populations surviving in
93 the Pacific Northwest [10].
94 Tree decays and compartmentalisation of decays are robust diagnostic criteria
95 for EIDs [11] Due to the importance of decays to the overall health status of a
96 tree, numerous drilling approaches have been suggested for assessing the
97 internal structure of trees and detecting hidden cavities [12], [13]. Although
98 drilling methods are accurate and reliable, nonetheless, destructive techniques

99 can cause irreversible damage to the tree, making it more vulnerable to fungi,
100 pathogens and pests. In addition, drilling methods are constrained to a single
101 point and fail to provide a coherent and comprehensive image of the internal
102 structure of the trunk. Within that context, there is an on-going call for novel
103 detection approaches and modern diagnostic tools [2], capable of detecting early
104 decay in an efficient and practical manner.

105 Non-destructive testing (NDT) for wood monitoring [14] is a suitable candidate
106 for detecting early decays in tree-trunks and their components (e.g., tree roots
107 [15], [16], [15]). NDT provides with a robust set of tools that can map the
108 internal structure of trees without disturbing its layers. The most mainstream
109 amongst the NDT techniques -applied for forestry applications- is the electrical
110 resistivity [16] and the ultrasound tomography [17]. Both of these methods can
111 effectively assess the health condition of a tree. Nonetheless, the measurement
112 configurations of these techniques make them unattainable for large-scale
113 forestry applications in which numerous trees have to be assessed in a short
114 period of time.

115 To tackle this, common-offset (CO) ground-penetrating radar (GPR) has been
116 suggested as an efficient and practical approach for tree monitoring [18]. To that
117 extent, a technique based on the interpretation of B-Scans in polar coordinates is
118 described in [19], [20], a layer-based detection is presented in [21] and a
119 hyperbola fitting approach is discussed in [18]. Apart from signal processing
120 approaches, tomographic methods are particularly appealing for tree monitoring
121 applications due to the fact that the measurements are taken on a closed surface
122 using a dense configuration. Microwave tomography tuned for cylindrical host
123 media has been extensively applied for column investigations [22] and

biomedical applications [23]. Furthermore, tomographic approaches based on the Born approximation and subject to CO-GPR configurations have shown promising results when applied for tree monitoring and early decay detection [24]. However, the resulting image may still be corrupted by artefacts, decreasing the signal-to-clutter ratio and reducing the reliability of the final results [24].

Migration is a mainstream processing tool that has been applied for both seismic and GPR applications in an effort to focus the received signal and increase the overall signal-to-clutter ratio [25]. The minimum computational requirements combined with its accuracy, have made migration one of the most extensively used approaches amongst GPR practitioners with a wide range of applications ranging from landmine detection [26], [27] to topography mapping [28]. Regarding forestry applications, a hyperbola summation -that resemblances Kirchhoff migration- has been suggested for tree measurements in [29]. In contrast to typical migration schemes applied to GPR [25], the approach described in [29] is not constrained to clinical half-spaces and thus, it can be applied in a straightforward manner to any arbitrary topography. Although preliminary laboratory results are promising [29], nonetheless real-field case studies are necessary in order to provide concrete evidences regarding the applicability of GPR for decay detection.

1.1 Statement of the Problem

CO-GPR has the potential to answer the on-going call for the modernization of detection tools for arboriculture applications. In order for GPR to be established as a mainstream forestry tool, processing methods have to be fine-tuned

accordingly and subsequently be subjected to a rigorous validation process. To that extent, numerical models and laboratory experiments can provide useful insights on the accuracy and efficiency of each investigated technique. Nonetheless, numerical and laboratory data can widely deviate from real field case studies and thus lead to an overestimation of the capabilities of GPR. Real-field case studies, although essential, are often unattainable due to practical considerations. In particular, a proper arboriculture case study should involve a diseased tree that is going to be cut down after the completion of the measurements. Furthermore, the fallen tree has to be cut into several slices in order to get an insight on its internal structure for validation purposes. The aforementioned procedure requires a dedicated and properly trained group of foresters that is often not available.

1.2 Aims and Objectives

In the current paper, we present a more efficient and less time-consuming focusing approach (compared to [29]) that is based on reverse-time (RT) migration [30]. In particular, the method described in [29] is a hyperbola summation that requires extensive 2D interpolations within the B-Scan. This results to large computational requirements especially when applied to 3D measurements. RT migration is particularly appealing for tree measurements due to its minimum computational requirements and its flexibility when it comes to rough topography. The most computationally intensive part of RT migration is an inverse fast Fourier transform which, can be executed in real-time in typical computers. The suggested scheme is successfully validated using both synthetic data and a real-field case study that involves a diseased urban tree within the

174 greater London area, UK. The proposed methodology was proven capable of
175 detecting decay of various sizes within the resolution of the employed antenna.
176 The current case study provides concrete evidences that GPR has the potential to
177 become an efficient tool for forestry and arboriculture applications.
178 The paper is organised as follows. Section 2 describes the theoretical
179 background of the RT migration as well as the processing pipeline that was
180 preliminarily employed. In addition to this, the positioning framework suggested
181 in [15] is discussed for the sake of consistency with presented results. Section 3
182 presents the numerical and real-field case studies accompanied with a detailed
183 discussion on the results. Lastly, the conclusions are drawn in Section 4.

184 ## 2. Methodology

185
186 The proposed methodology consists of four distinct stages, namely, A) data
187 positioning, B) pre-processing, C) migration and D) post-migration smoothing
188 (see Figure 1). In the first step, the measurements are positioned along the
189 surface of the trunk using an arc length parameterization. Subsequently the raw
190 data are processed in order to eliminate unwanted clutter and ringing noise. The
191 first two steps are not sequential and thus the order can be reversed. The
192 processed B-Scan is then migrated. Lastly, a smoothing filter is applied in order
193 to eliminate migration artefacts. Notice that all the aforementioned steps require
194 minimum computational requirements and can be executed in almost real-time
195 using conventional mainstream computers.

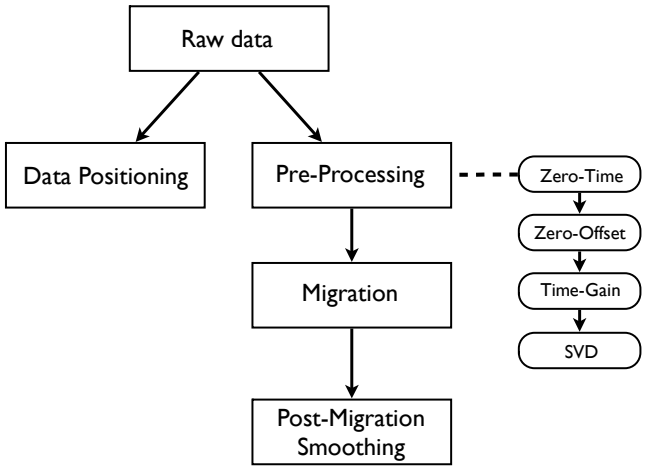

Figure 1: Flowchart describing the proposed processing framework. (No colour in print)

2.1 Positioning Scheme

Typical CO-GPR systems position each A-Scan based on a wheel-measuring device that associates every received signal output with its associate position. This configuration was designed for line measurements subject to flat surfaces and fails to compensate for irregular topographies. Regarding tree surveys, it is known that measurements are collected on a highly irregular surface. Thus, prior to any processing approach, each A-Scan should be accurately positioned along the investigated surface. To that extent, in order to convert the measured distance (from the wheel-measuring device) to its corresponding coordinates, we employ an arc-length parameterisation [31], [32], initially described in [18].

The first step of the arc-length parameterisation is to digitize the investigated surface using a sufficient (n) number of points along the surface of the trunk $\mathbf{x},\mathbf{y} \in \mathbb{R}^n$. Subsequently, the vector $\mathbf{t} \in \mathbb{R}^n \mid 0 < t < 1$ is defined, which is going to be used for the parametric representation of the shape of the tree [18]. A spline interpolation is subsequently used in order to map the vectors $(\mathbf{x}, \mathbf{t})$ and $(\mathbf{y}, \mathbf{t})$ to the continuous scalar functions $P(t)$ and $Q(t)$ respectively. Notice that the bounds of $\mathbf{t}$ do not affect the final output since the coefficients of the fitted polynomial

are adjusted accordingly. The position vector $\mathbf{F} = [P(t), Q(t)]$ represents the shape of the tree with respect to the arbitrary value *t*. The arc-length (*s*) of the positional vector **F** throughout the vector **t** is given by

$$s(\tau) = \int_0^\tau \left|\left|\frac{d\mathbf{F}}{dt}\right|\right| dt = \int_0^\tau \sqrt{\left(\frac{dP(t)}{dt}\right)^2 + \left(\frac{dQ(t)}{dt}\right)^2}\, dt \quad . \quad (1)$$

where $\tau \in [0,1]$ is a continuous variable along the boundaries of the arbitrary vector **t.** The integral in (1) is evaluated numerically [15] using different τ values varying from [0,1]. A spline interpolation is then used in order to map the values of τ with respect to the distance *s.* Thus, the distance can now be expressed in a continuous manner with respect to *t.* Consequently; the position vector can now be expressed with respect to the distance $\mathbf{F} = [P(t(s)), Q(t(s))]$. This implies that the position of the antenna can now be calculated based on the distance (*s*) measured using a typical wheel-measuring device [18].

2.2 Pre-Processing

Prior to the RT migration, the raw B-Scan has to be carefully processed in order to transform the data in a suitable format for the following processing stages. The processing pipeline applied in this paper -similar to [18]- consists of four sequential steps:

- *Time-zero removal:* in this step, the starting time t_0 of the pulse is estimated and the signal prior to t_0 is deleted. This step is particularly important since the estimated time-zero greatly affects the performance of the RT migration. The first peak of the derivative of the A-Scan with respect to time is chosen to represent the time-zero in the current paper.

- *Zero-offset removal:* in this step, static phenomena that corrupt the received A-Scans are removed by fitting a second order polynomial to the received signal [33].
- *Time-varying gain:* an incremental gain is applied in order to compensate for the losses present within the trunk.
- *Singular value decomposition:* trees are complex media that consist of distinct layers with different compositions and dielectric properties [18]. Due to the layered nature of trees, the raw B-Scan is corrupted with ringing noise that masks the reflections from the decay and reduces the overall signal-to-clutter ratio [18]. To tackle this, a singular value decomposition (SVD) filter (similar to [18]) is applied here. The raw B-Scan is treated as a 2D matrix $\mathbf{B} \in \mathbb{R}^{w \times v}$ where *w* and *v* are the number of measurements and the number of time-steps, respectively. The matrix **B** is then decomposed via $\mathbf{B=UMV^T}$, where **U** and **V** are the orthogonal matrices that contain the left and right singular vectors of **B.** The matrix **M** is a square matrix that contains the singular values of **B.** These singular values are placed in a decreasing order along the main diagonal of **M.** The rationale behind the application of the SVD filter is that large singular values are typically related to dominant periodic patterns arising from the repetitive reflections between the tree layers [18]. Thus, setting the dominant singular values to zero and subsequently reconstructing the matrix **B** will result to a revised B-Scan with a lower number of features associated with ringing noise [18]**.** The number of dominant singular values to be filtered out is usually <10. This number is a hyperparameter that it is tuned via a trial and error procedure.

The above processing pipeline is tested in the numerical case study shown in Figure 2. A generic hardwood consisted with four layers is simulated using the finite-difference time domain (FDTD) method [34], [35], [36] (more details on the numerical simulations are given in Section 3). An early decay is simulated as a hollow chamber within the sapwood. The raw and the processed data are shown in Figure 3. The static components and the signal prior to time-zero are initially removed. Subsequently, a linear gain is applied to each A-Scan. Lastly, an SVD filter, filtering out the three most dominant eigenvalues, is applied to the data. From Figure 3, it is apparent that the employed processing approach [18] can effectively remove the ringing noise and can enhance the reflections from the early decay.

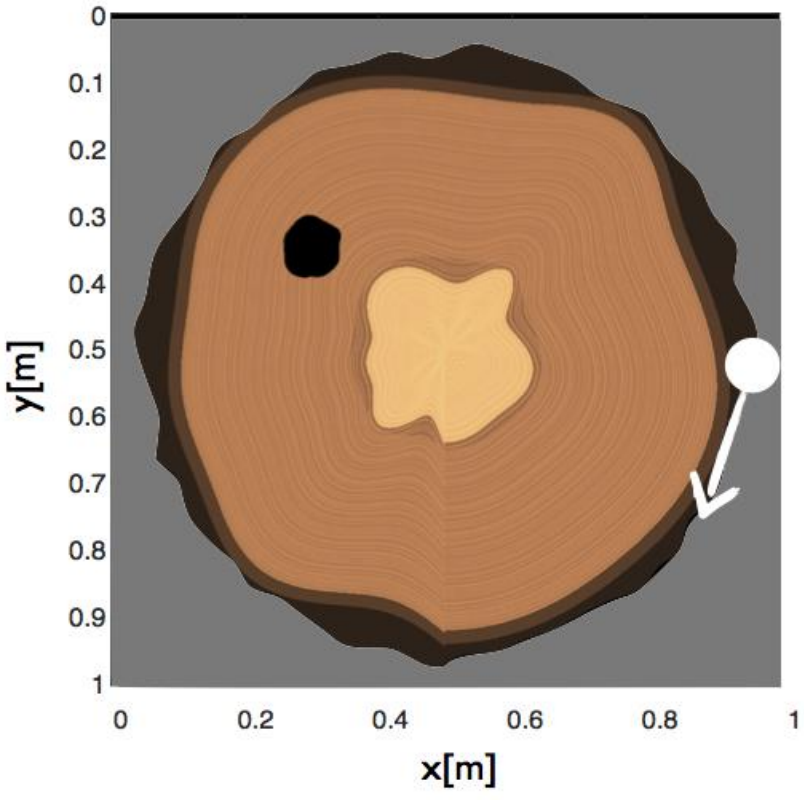

Figure 2: A numerical case study for the investigation of the received signal of an early decay in a generic hardwood scenario. The white dot represents the starting point of the scan and the arrow shows the direction of the measurements. (No colour in print)

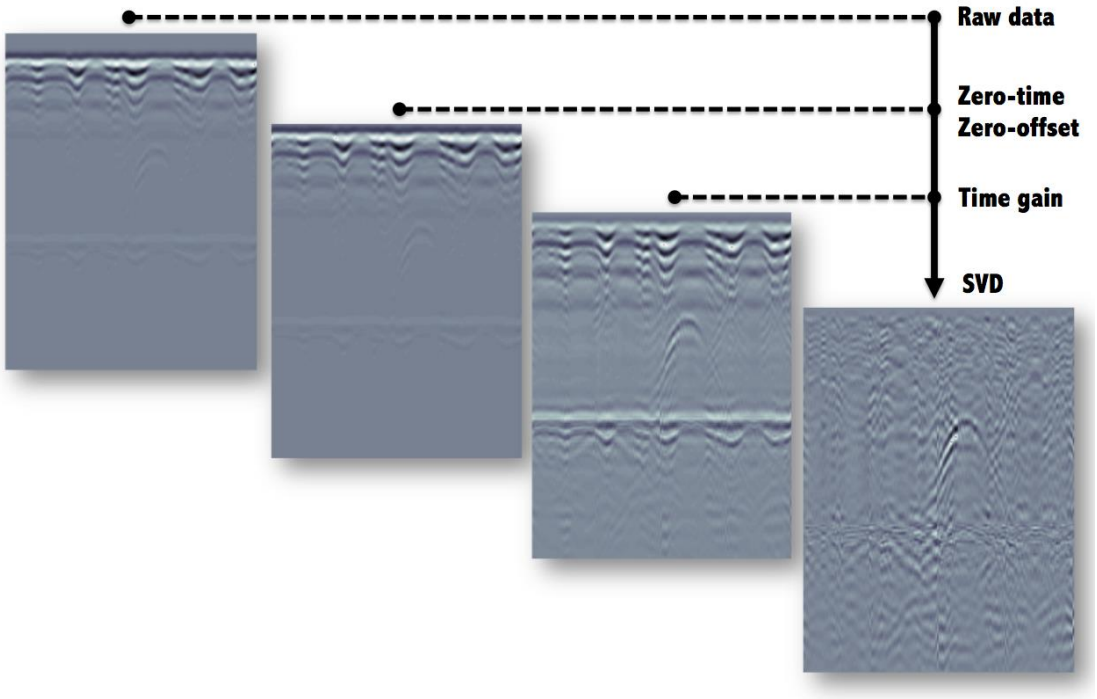

Figure 3: The employed processing pipeline applied to the simulated data from the case study illustrated in Figure 2. (No colour in print)

2.3 Reverse Time Migration

RT migration using monostatic measurement configurations is based on the exploding reflector model [30]. This model approximates every scatterer with an equivalent source that is excited when the incident wave reaches the investigated target. The equivalent sources radiate towards the position of the antenna following the same path as the incident field [30]. Thus, reversing the received signals with respect to time and use them as excitation sources along **F** will result to a radiated electromagnetic field collapsing at the coordinates of the scatterers as time approaches to zero. To compensate the two-way travel time, the velocity of the medium during the back-propagation is set to half the actual velocity [30]. The mathematical formulation for the RT migration in homogenous media is

$$E_s(\mathbf{r}_m,\omega) = k_b^2 \int_0^M g_e\left(\mathbf{r}_m,\mathbf{F}(s),\omega\right) E_{inc}(\mathbf{F}(s),\omega) ds \quad (2)$$

where E_s is the back-propagated field in the frequency domain, $\mathbf{r}_m$ is the parameter indicating the coordinates within the trunk, ω is the angular velocity, k_b is the wavenumber assuming a homogenous velocity (half of the actual velocity), E_{inc} is the reversed received signal after processing, *M* is the circumference of the trunk and g_e is the Green's function for a homogenous space. The Green's function in the frequency domain equals with

$$g_e\left(\mathbf{r}_m,\mathbf{F}(s),\omega\right) = \frac{j}{4} H_0^2\left(k_b||\mathbf{r}_m - \mathbf{F}(s)||\right) \quad (3)$$

where $j = \sqrt{-1}$ and H_0^2 is the Hankel function of the second kind and zero order [24]. The migrated image is estimated after applying the inverse Fourier transform to E_s and subsequently set *t = 0.*

It should be noted that the exploding model on which migration is based on, does not take into account the presence of repetitive reflections between the tree layers. Therefore, a non-adequate elimination of the ringing noise will result to shallow artefacts due to the misinterpretation of the ringing noise as fictitious scatterers.

2.4 Post-migration processing

The post-migrated image is subsequently subjected to image processing in order to remove migration effects and enhance the quality of the signal. The resulting migrated image is initially squared and subsequently convolved with a 2D homogenous Gaussian function

$$G(x,y) = \frac{1}{2\pi\sigma^2} e^{-\frac{x^2+y^2}{2\sigma^2}} \quad (4)$$

where σ is a unit-less variable that controls the intensity of the filter [37].

Table 1: The extended Debye properties of the tree layers used for the numerical simulations [17].

Tree Section Component	Water Content [%]	ε_∞	$\Delta\varepsilon$	σ [$W^{-1}m^{-1}$]	t_0 (psec)
Cambium layer	70	9	43	1	9.23
Outer sapwood	30	6.1	12.36	0.033	9.23
Inner sapwood	25	5.9	9.66	0.02	9.23
Rings	10	5.4	3.1	0.0083	9.23
Heartwood	5	5.22	1.43	0.005	9.23
Bark	0	5	0	0	9.23

3. Case Studies and Results

3.1 Numerical Case Study

In the current section, the proposed detection framework is tested using synthetic but nonetheless realistic data. An FDTD method is used for the simulations with a second order accuracy in both space and time [34], [35], [36]. The spatial discretisation step is set to $\Delta x = \Delta y = \Delta z = 1$ mm and the time increment is chosen based on the Courant limit [34]. Regarding the excitation of the system, a numerical equivalent of the commercial antenna GSSI 1.5 GHz [33] is used for the simulations. Simulating the antenna in different positions along the curved surface of the trunk requires the implementation of tilted excitation sources. These scenarios give rise to numerical errors and instabilities due to the constraints from the orthogonal grid of FDTD. To overcome this, instead of moving the antenna along the trunk, the trunk is rotated while the transducer remains still [18].

342 The numerical case study examined in this Section is a generic semi-saturated
343 hardwood. The simulated trunk consists of five distinct layers i.e. the bark, the
344 cambium layer, the outer-sapwood, the inner-sapwood and the heartwood. The
345 dielectric properties of the layers are estimated using a complex-refractive index
346 model (CRIM) [18] subject to the volumetric fraction of water expected in each
347 layer [18]. Subsequently, in order for the dielectric properties to be compatible
348 with FDTD, the complex permittivity is approximated with an extended Debye
349 model (see Table 1) [18], [38]. Lastly, two decays with different sizes are
350 incorporated within the outer-sapwood (see Figure 4). The decays are simulated
351 as hollow semi-cylindrical objects with their main axis being parallel to the main
352 axis of the trunk.
353 The raw B-Scan is initially subjected to the pre-processing pipeline described in
354 Section 2.2. Subsequently, the revised traces are reversed with respect to time
355 and used as input sources in equation (2). The bulk permittivity of the medium is
356 set to $\varepsilon=16$. The migrated image is then squared and subsequently smoothed
357 using a Gaussian filter (kernel size equals to 30 and σ = 15). Figure 5 illustrates
358 the migrated image and the post-migration processing steps. Moreover, Figure 6
359 shows the effect of σ on the final outputs. Increasing σ results to a low-pass filter
360 that decreases migration artefacts and high frequency noise. Both of the decays
361 are accurately detected indicating the validity of the suggested methodology.
362 From Figure 5 is apparent that the relative size between the decays can be
363 extracted from the reconstructed image. Evidences are also given regarding the
364 presence of heartwood at the centre of the trunk.
365

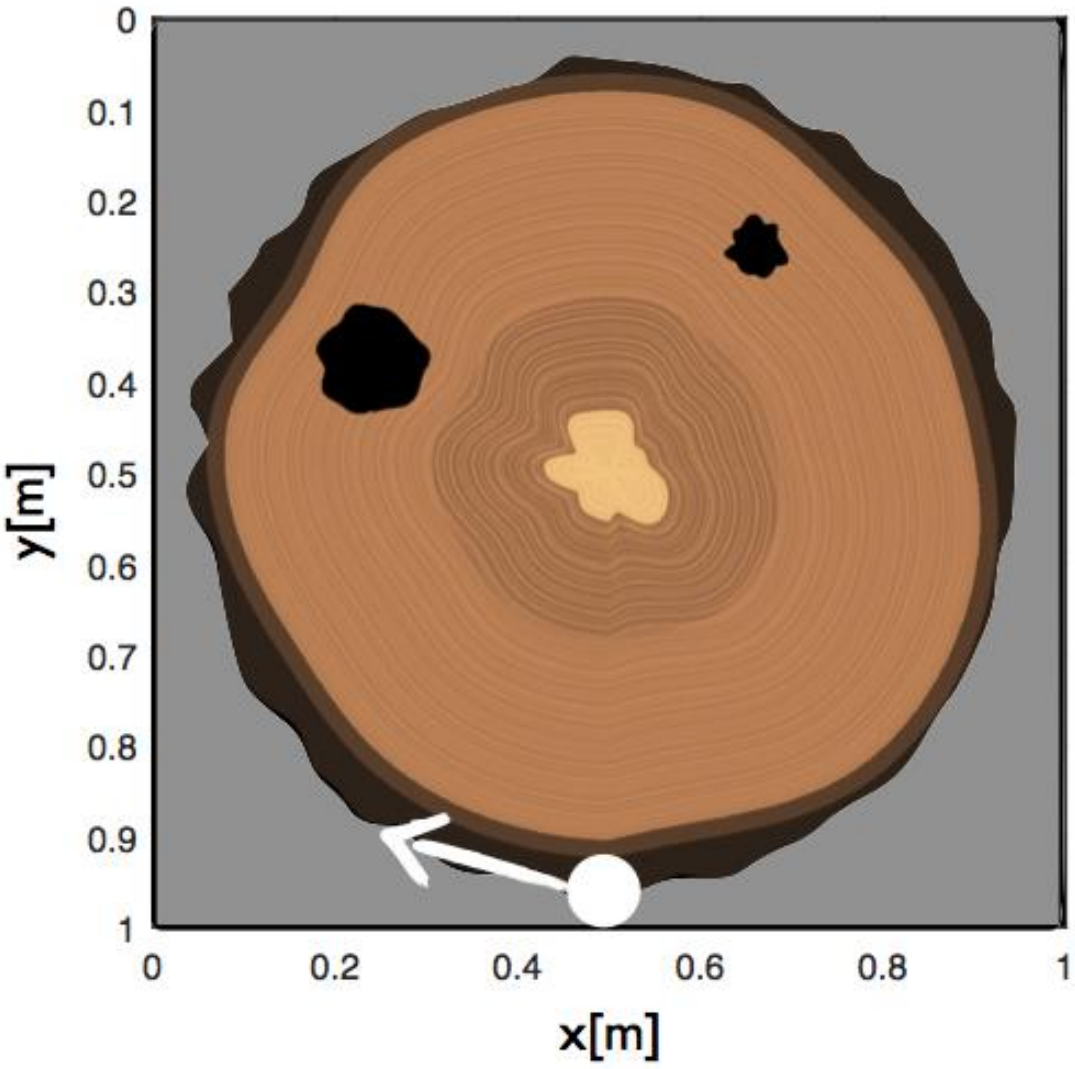

Figure 4: A numerical case study for the investigation of the received signal of two early decays in a generic hardwood scenario. The white dot represents the starting point of the scan and the arrow shows the direction of the measurements. (No colour in print)

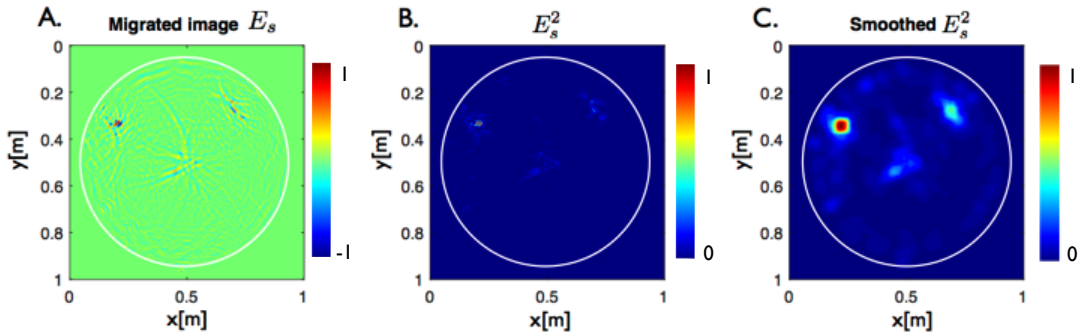

Figure 5: The reconstructed internal structure of the synthetic trunk shown in Figure 4.A) The resulting image using RT migration. B) Squaring the migrated image in order to increase the overall signal-to-clutter ratio. C) A Gaussian blur filter is applied in order to remove the migration-effects. The line of measurements is assumed circular to make the case study more realistic and challenging. (No colour in print)

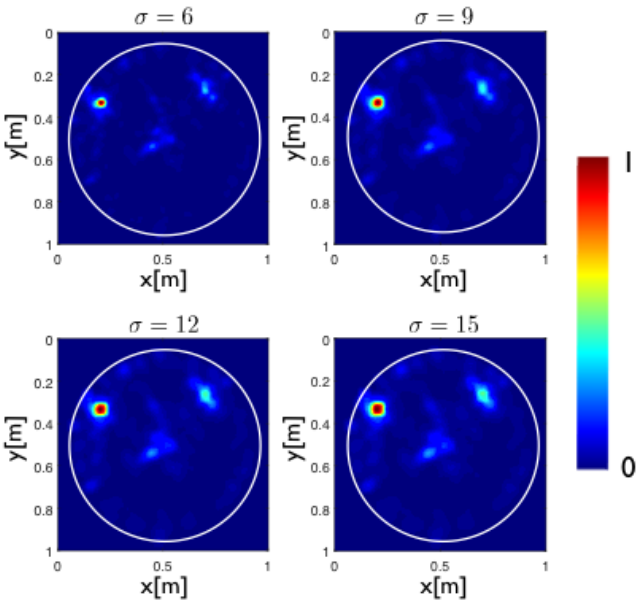

Figure 6: The effect of σ to the resulting reconstructed image. Increasing σ results to low pass filter that filters out high frequency noise and migration artefacts. (No colour in print)

3.1 Field Measurements

The proposed detection scheme is now tested in a real-field case study from a diseased tree located at Gunnersbury Park, London, UK (see Figure 7). The employed antenna for this experiment was the dual-polarised hand-held antenna "Aladdin" from IDS GeoRadar (Part of Hexagon). The central frequency of "Aladdin" is 2 GHz, the time-step equals to dt = 6.25e−11 s and the spatial step of the measuring wheel is Δ = 1 cm. Circular scans were collected every 5 cm along the main axis of the tree and parallel to the ground. The overall scanned area is 1.35 m long and consists of 27 parallel circular scans. The inspected area has a semi-cylindrical shape with a varying circumference. The circumference of each section was accurately estimated and subsequently incorporated into the detection scheme by means of the measuring-wheel device attached to the antenna.

Prior to the measurements, the bulk permittivity of the trunk was estimated at $\epsilon \approx 30$. The permittivity was calculated based on the two-way travel time

needed for the wave to travel from one side of the trunk to the other. The permittivity measurements were conducted using the 1 GHz horn antenna system from IDS GeoRadar (Part of Hexagon). The high-directivity of the horn antenna made it possible to get a clear reflection from the back of the trunk. To further enhance the signal, a perfect conducting (PEC) sheet was attached to the tree.

After the completion of the measurements, the tree was torn down (see Figure 8) and cut into several slices in an effort to get an insight of its internal structure. From Figure 9, a dominant decay extending along the main axis of the trunk is clearly visible. The decay has an irregular shape and a sharp transition from the healthy sapwood. The diameter of the decay is approximately ~60 cm and does not show any dominant increasing or decreasing trend along the trunk.

Figure 10 illustrates the reconstructed image using the methodology described in Section 2. Every B-Scan is initially processed using a time-zero correction, a zero-offset removal, a linear gain and an SVD filter (five dominant eigenvalues are filtered out). Subsequently, an RT migration is applied to each processed B-Scan subject to a homogenous medium with $\epsilon = 30$. The migrated images are furthermore squared and smoothed using a Gaussian blur filter (kernel size equals to 30 and σ = 15). The resulting 2D images are then combined to create a pseudo-3D model of the trunk. From Figure 10, it is apparent that there are clear evidences of a major feature at the centre of the trunk extending along its main axis. This is in good agreement with the actual structure of the tree, shown in Figure 9. A reconstructed slice of the tree and its corresponding processed B-Scan are shown in Figure 11. The shape and the size of the decay are adequately

recovered. Discrepancies between the actual and the predicted shape are due to local variations of permittivity within the trunk that deviate from the assumption of a homogenous medium with $\varepsilon=30$.

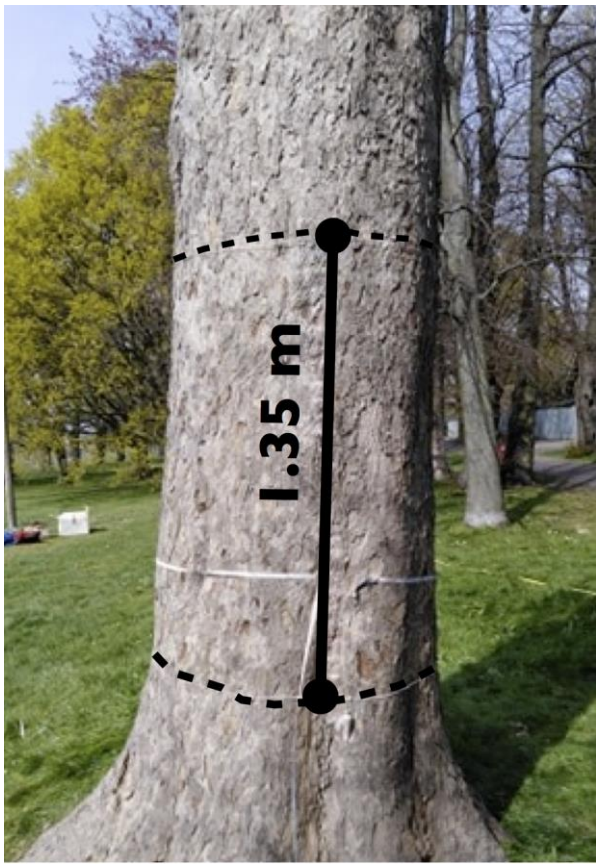

Figure 7: The investigated tree at Gunnersbury Park, London, UK. The scanned area is highlighted between the dotted lines. (No colour in print)

Figure 8: The investigated tree was torn down after the completion of the measurements in order to get an insight on its internal structure. (No colour in print)

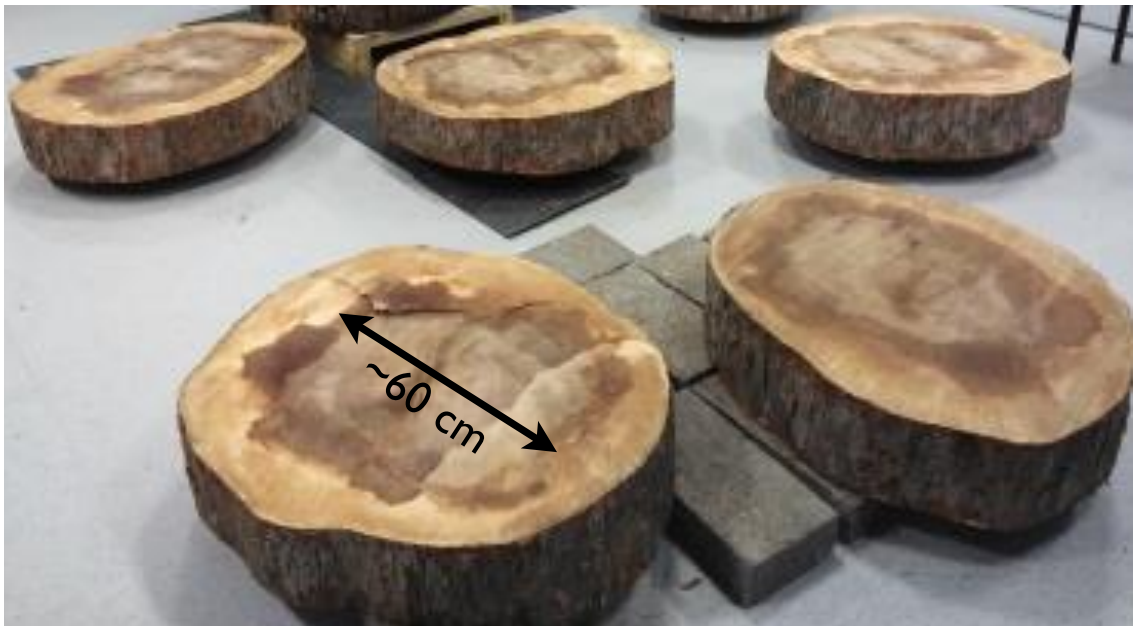

Figure 9: Slices collected from the investigated tree shown in Figure 7. A dominant decay (with a diameter of approximately ~60 cm) extending along the main axis of the trunk is clearly visible. (No colour in print)

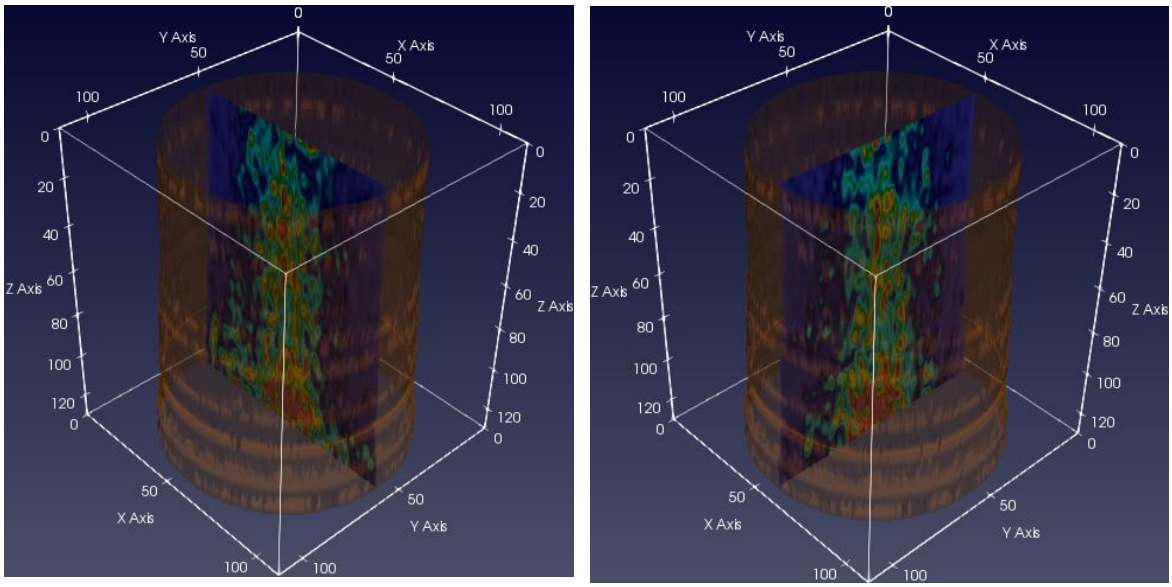

Figure 10: The reconstructed internal structure of the scanned area shown in Figure 7 using the processing scheme discussed in Section 2. The axis are in cm. (No colour in print)

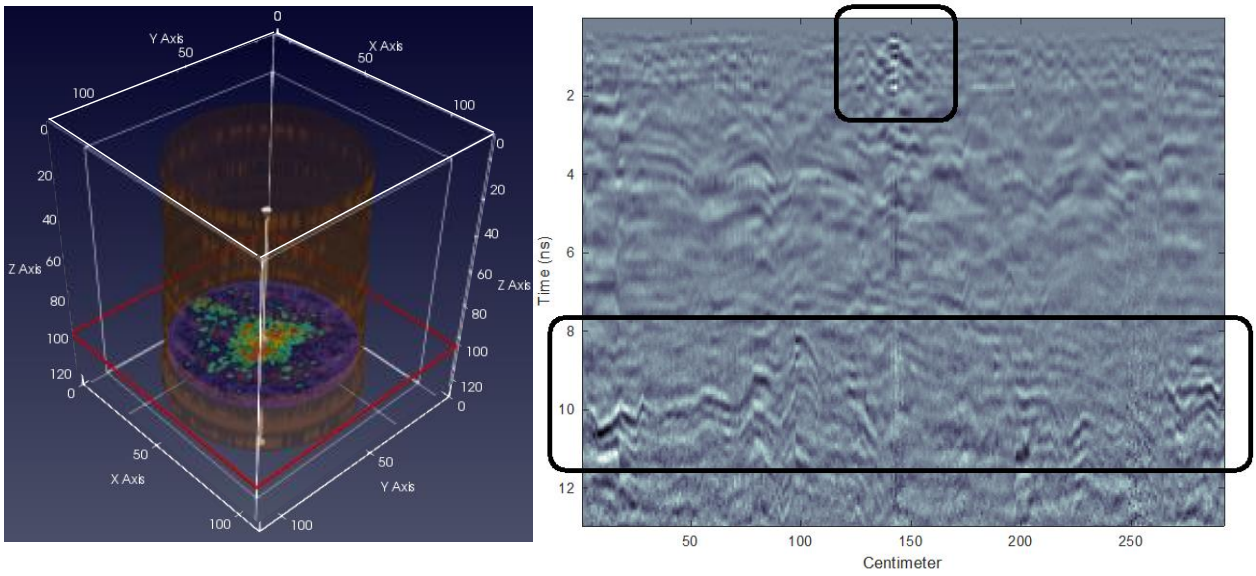

Figure 11: A reconstructed slice (left) and its corresponding processed B-Scan (right). Two main decay are apparent, one shallow with small size and one bigger one at the centre of the trunk. The reflections of the two decay are highlighted within the black boxes. (No colour in print)

4. Conclusions

In this paper, a detection framework is described fine-tuned for detecting hidden decay and cavities in diseased trees. The main advantage of the described methodology is that it can be applied in a straightforward manner using commercial ground-penetrating radar (GPR) antennas without the need for bespoke systems and complex measurement configurations. The processing pipeline of the scheme primarily consists of a singular value decomposition (SVD) filter coupled with a reverse-time (RT) migration. This implies that the suggested methodology has minimum computational and operational requirements making it particularly appealing for large-scale forestry applications. The accuracy of the described framework is rigorously tested via numerical and real-field case studies. The results clearly suggest that GPR coupled with the proposed methodology is a robust detection tool capable of assessing the health conditions of trees in an efficient and practical manner.

Consequently, GPR can answer the on-going call for efficient arboriculture tools and provide a viable alternative for tackling modern challenges related to emerging infectious diseases of trees. The proposed methodology has been validated using high frequency hand-held antennas. Future work will include the application of lower frequencies in an attempt to increase the penetration depth and the overall signal to clutter ratio. Lower frequency antennas are essential in order to overcome the electromagnetic losses within the trunk and can potentially increase the performance of the proposed methodology.

Acknowledgments

The authors would like to express their sincere thanks and gratitude to the following trusts, charities, organizations and individuals for their generosity in supporting this project: Lord Faringdon Charitable Trust, The Schroder Foundation, Cazenove Charitable Trust, Ernest Cook, Sir Henry Keswick, Ian Bond, P. F. Charitable Trust, Prospect Investment Management Limited, The Adrian Swire Charitable Trust, The John Swire 1989 Charitable Trust, The Sackler Trust, The Tanlaw Foundation and The Wyfold Charitable Trust.

This paper is dedicated to the memory of Jonathon West, a friend, a colleague, a forester, a conservationist and an environmentalist who died following an accident in the woodland that he loved.

References

[1] A. Broome, D. Ray, R. Mitchell and R. Harmer, ”Responding to ash dieback (Hymenoscyphus fraxineus) in the UK: woodland composition and replacement tree species,” *Forestry, An International Journal of Forest Research*, vol. 92, pp. 108–119, 2019.

[2] A. Santini, L. Ghelardini, C. De Pace, [...] and J. Stenlid, ”Biogeographical patterns and determinants of invasion by forest pathogens in Europe,” *New Phytologist*, vol. 197, pp. 238-250, 2012.

[3] A. M. Ellison, M. S. Bank, B. D. Clinton, [...] and J. R. Webster, ”Loss of foundation species: consequences for the structure and dynamics of forested ecosystem,” *The Ecological Society of America*, vol. 3, pp. 479-486, 2005.

[4] S. A. Anagnostakis, ”Chestnut blight: the classical problem of an introduced pathogen,” *Mycologia*, vol. 79, pp. 23-37, 1987.

[5] Q. Guo, M. Rejmanek and J. Wen, ”Geographical, socioeconomic and ecological determinants of exotic plant naturalization in the United States: insights and updates from improved data,” *NeoBiota*, vol. 12, pp. 41-55, 2012.

[6] J. J. Stocks, R. J. A. Buggs and S. J. Lee, ”A first assessment of Fraxinus excelsion (common ash) susceptibility to Hymenoscyphus fraxineus (ash dieback) throughout the British Isles,” Nature, Scientific Reports, vol. 7, 2017.

[7] R. Worrell, “An Assessment of the Potential Impacts of Ash Dieback in Scotland,” Available online: https: //bit.ly/2ZkYhNc (accessed on 30 August 2019)

[8] N. Brown, “Epidemiology of Acute Oak Decline in Great Britain,” Available online: https://spiral.imperial.ac. uk/handle/10044/1/30827 (accessed on 30 August 2019).

[9] S. Denman, N. Brown, S. Kirk, M. Jeger and J. Webber, ”A description of the symptoms of Acute Oak Decline in Britain and a comparative review on causes of similar disorders on oak in Europe,” *Forestry*, vol. 87, pp. 535-551, 2014.

[10] A. M. Ellison, M. S. Bank, B. D. Clinton, [...] and J. R. Webster, ”Loss of foundation species: consequences for the structure and dynamics of forested ecosystem,” *The Ecological Society of America*, vol. 3, pp. 479-486, 2005.

[11] W. C. Shortle and K. R. Dudzik, *Wood Decay in Living and Dead Trees: A Pictorial Overview*, U.S. FOREST SERVICE, 2012.

[12] P.M.W.Xu and R.Wimmer,”Application of a drill resistance technique for density profile measurement in wood composite panels,” *Forest Prod. J.*, vol. 45, pp. 90-93, 1995.

[13] W. Moore, ”The combined use of the RESISTOGRAPH and the Shigometer for the accurate mapping and diagnosis of the internal condition of wood support orangs of trees,” *Arboricultural J.*, vol. 23, pp. 273–287, 1999.

[14] V.Bucur. *Nondestructive Characterization and Imaging of Wood.* Berlin, Germany: Springer, 2003.

[15] Lantini, L., Holleworth, R., Egyir, D., Giannakis, I., Tosti, F., and Alani, A.M. (2018). Use of Ground Penetrating Radar for Assessing Interconnections between Root Systems of

534 Different Matured Tree Species. In: Proc of the IEEE International Conference on Metrology
535 for Archaeology and Cultural Heritage (MetroArchaeo 2018), Cassino, Italy, October 22-24,
536 2018.

537 [16] A. Guyot, K.T. Ostergaard, M. Lenkopane, J. Fanand, D.A. Lockington, "Using
538 electrical resistivity tomography to differentiate sapwood from heartwood: application to
539 conifers," *Tree Physiology*, vol. 33, pp. 187– 194, 2013.

540 [17] C. J. Lin and T. H. Yang, "Detection of acoustic velocity and electrical resistance
541 tomographies for evaluation of peripheral-inner wood demarcation in urban royal palms,"
542 *Urban Forestry and Urban Greening*, vol. 14, pp. 583-589, 2015.

543 [18] I. Giannakis, G. Tosti, L. Lantini and A. Alani, "Health monitoring of tree-trunks using
544 ground penetrating radar," *IEEE Transactions on Geoscience and Remote Sensing,* vol. 57,
545 no. 10, pp. 8317-8326, 2019.

546 [19] J. Jezova, L. Mertens and S. Lambot, "Ground-penetrating radar for observing tree
547 trunks and other cylindrical objects," *Construction and Building Materials*, vol. 123, pp. 214–
548 225, 2016.

549 [20] J. Jezova, J. Harou and S. Lambot, "Reflection waveforms occurring in bistatic radar
550 testing of columns and tree trunks," *Construction and Building Materials,* vol. 174, pp. 388-
551 400, 2018.

552 [21] X. Xiao, J. Wen, Z. Xiao and W. Li, "Detecting and measuring internal anomalies in tree
553 trunks using radar data for layer identification," *Journal of Sensors*, vol. 2018, pp. 1-11,
554 2018.

555 [22] G. Leucci, N. Masini, R. Persico and F. Soldovieri, "GPR and sonic tomography
556 for structural restoration: The case of the cathedral of Tricarico," *J. Geophys. Eng.*
557 vol. *8*, pp. S76–S92, 2011.

558 [23] M. Pastorino, *Microwave Imaging*, John Wiley & Sons, Inc.: Hoboken, NJ, USA,
559 2010.

560 [24] A. M. Alani, F. Soldovieri, I. Catapano, I. Giannakis, G. Gennarelli, L. Lantini, G.
561 Ludeno and F. Tosti, "The Use of Ground Penetrating Radar and Microwave Tomography for
562 the Detection of Decay and Cavities in Tree Trunks," *Remote Sensing*, 2019.

563 [25] D. J. Daniels, *Ground* Penetrating *Radar*, 2nd ed. London, U.K.: Institution of
564 Engineering and Technology, 2004.

565 [26] J. Schofield, D. Daniels and P. Hammerton, "A Multiple Migration and Stacking
566 Algorithm Designed for Land Mine Detection," *IEEE Transactions on Geoscience and*
567 *Remote Sensing,* vol. 52, no. 11, pp. 6983-6988, 2014.
568
569 [27] M. A. Gonzlez-Huici, I. Catapano and F. Soldovieri, "A Comparative Study of GPR
570 Reconstruction Approaches for Landmine Detection," *IEEE Journal of Selected Topics in*
571 *Applied Earth Observations and Remote Sensing*, vol. 7, no. 12, pp. 4869-4878, 2014
572

573 [28] X. Feng, M. Sato, C. Liu and Y. Zhang, "Profiling the Rough Surface by Migration,"
574 *IEEE Geoscience and Remote Sensing Letters*, vol. 6, no.2, pp. 258-262, April 2009.

[29] I. Giannakis, F. Tosti, L. Lantini, D. Egyir and A. M. Alani, "Signal Processing For Tree-Trunk Investigation Using Ground Penetrating Radar," in *Proc. Of 10th Workshop on Advanced Ground Penetrating Radar,* Netherlands, 2019.

[30] C. J. Leuschen and R. G. Plumb, "A matched-filter-based reverse-time migration algorithm for ground-penetrating radar data," *IEEE Transactions on Geoscience and Remote Sensing*, vol. 39, no. 5, pp. 929-936, 2001.

[31] R. J. Sharpe and R. W. Thorne, "Numerical method for extracting an arc length parameterization from parametric curves," *Comput.-Aided Des.,* vol. 14, no. 2, pp. 79–81, 1982.

[32] B. Guenter and R. Parent, "Computing the arc length of parametric curves," *IEEE Comput. Graph. Appl.*, vol. 10, no. 3, pp. 72–78, 1990.

[33] I. Giannakis, A. Giannopoulos, and C. Warren, "Realistic FDTD GPR antenna models optimized using a novel linear/nonlinear full- waveform inversion," *IEEE Trans. Geosci. Remote Sens.*, vol. 57, no. 3, pp. 1768-1778, Mar. 2019.

[34] A. Taflove and S. C. Hagness, *Computational Electrodynamics: The Finite-Difference Time-Domain Method*, 2nd ed. Norwood, MA, USA: Artech House, 2000.

[35] C. Warren, A. Giannopoulos, and I. Giannakis, "gprMax: Open source software to simulate electromagnetic wave propagation for ground penetrating radar," *Comput. Phys. Commun.*, vol. 209, pp. 163–170, Dec. 2016.

[36] C. Warren *et al.*, "A CUDA-based GPU engine for gprMax: Open source FDTD electromagnetic simulation software," *Comput. Phys. Commun.*, vol. 237, pp. 208-218, Apr. 2019.

[37] S. M, Nixon and A. S. Aguado. *Feature Extraction and Image Processing for Computer Vision*. Academic Press, 2008.

[38] D. F. Kelley, T. J. Destan, and R. J. Luebbers, "Debye function expansions of complex permittivity using a hybrid particle swarm-least squares optimization approach," *IEEE Trans. Antennas Propag.*, vol. 55, no. 7, pp. 1999–2005, 2007.